Analysis of thermally-induced displacements of the HartRAO Lunar Laser Ranger optical tube: its impact on pointing

Philemon Tsele[1],* Ludwig Combrinck[1], Roelf Botha[2], Bongani Ngcobo[2]

[1]Department of Geography, Geoinformatics and Meteorology, University of Pretoria, Pretoria 0002, South Africa

[2]Space Geodesy Programme, South African Radio Astronomy Observatory, P.O. Box 443, Krugersdorp, 1740 South Africa

*Corresponding author: philemon.tsele@up.ac.za

DOI: http://dx.doi.org/10.4314/sajg.v12i.2.8

Abstract

The Hartebeesthoek Radio Astronomy Observatory (HartRAO) of South Africa is developing a Lunar Laser Ranging (LLR) system to achieve sub-centimetre range precision to the Moon. Key to this high precision expectation, which includes improving the overall operational performance of its telescope, is the thermal analysis of the telescope structure. In this study, thermal sensors were mounted on the thermally- important areas of the tube structure to measure the tube displacements emanating from the varying ambient air temperatures. A laser distance-measurement system was used for this purpose. Results showed that while the optical tube undergoes structural changes with changes in temperature, the tube position closer to the place where the spider assembly is mounted is unevenly displaced in three directions. In particular, for the time period considered in this study, it was found that the relative displacements on average at prisms 1, 2 and 3 in the vertical direction were 2.5540 ± 0.0007 m, 1.3750 ± 0.0008 m and 1.9780 ± 0.0007 m, respectively. The corresponding standard deviation (SD) values of ±0.0007 m, ±0.0008 m and ±0.0007 m denotes the average deviations that occurred in the vertical direction at the centre of prisms 1, 2 and 3, respectively. The generally higher SD of relative displacements in the vertical direction rather than in the easting and northing directions, suggest that the tube experienced greater variations in the vertical direction. Furthermore, the lower arc of the tube front, was found to have increased variability, and therefore it was hypothesised to introduce more elevation pointing offsets than azimuth for the LLR. This information constitutes an important input for guiding the efforts to determine the extent of the correction needed to be fed into the LLR telescope pointing model to counteract expected thermally induced pointing offsets.

1. Introduction

One of the key considerations for the scientific performance of a ground-based telescope, is the thermal analysis of the composite structure of the telescope and the associated optics, which are based on the thermal properties of its component materials and its interaction with the varying local climatic environment (Wang et al., 2018). It is an experimental fact that classical telescopes built from materials such as aluminium alloys and steel are subject to varying dimensional changes owing to temperature variations (Bely, 2003). Thus, a thorough understanding of the thermal environment of the telescope observatory site, the properties of the component materials, and the systemic performance requirements of the telescope could be essential for determining appropriate modeling procedures and mitigation strategies to deal with temperature variations. In addition, temperature variations have also been shown to have an effect on the overall pointing error, especially for unhoused or open-air telescopes (Baars et al., 1988; Énard et al., 1996; Ukita, 1999; Greve and MacLeod, 2001; Shinnaga et al., 2004; Wresnik et al., 2007; Mittag et al., 2008; Cho et al., 2010; Pisanu et al., 2010; Vogiatzis, 2010).

Several studies have demonstrated that a reliance solely on passive measures, such as the coating and insulation of the component materials, to constrain the thermal effects arising from heat transfer mechanisms (Çengel and Ghajar, 2011) may not yield desirable results, especially under extreme and rapid ambient climatic changes (Ukita, 1999). Alternatively, active measures have proven to be reliable in providing detailed thermally-induced pointing errors in respect of (real-time) temperature monitoring and modeling. Such measures entail the installation of several temperature sensors at strategically identified locations over the entire structure of the telescope. Temperature measurements can thus be acquired and subsequently analyzed in order to (i) monitor thermal variations and consequent deformations in the composite structure of the telescope, (ii) estimate the magnitude of the thermally-induced displacements of the critical components so as to determine the amount of correction that would be necessary to counteract the thermally-induced pointing offsets, and (iii) guide the development of a robust thermal model for mitigating the thermal variations of the critical telescopic elements, such as the tube and mirrors (Ukita, 1999; Mittag et al., 2008; Pisanu et al., 2010; Bremer and Penalver, 2002; Greve et al., 2005; Murphy Jr et al., 2008; Greve and Kaercher, 2009; Tsela et al., 2016b). In particular, the coupling of the acquired temperature measurements with observations from the associated inclinometers and distance-measurement laser systems has also shown the potential to determine structural displacements, that are based on varying amounts of the incidental beam drift (Hu et al., 2015; Cui et al., 2015; Cui et al., 2016), and correlations between the pointing error and thermally-induced deformation in respect of the selected structural components of the telescope (Pisanu et al., 2010). Overall, these studies confirm to a reasonable degree that the thermal analysis of an open-air, ground-based telescope in particular, may be necessary but that it should take into account the structural

design of the telescope, the thermal properties of the component materials, and the variability of the site-specific climatic factors.

The Lunar Laser Ranger (LLR) based at the Hartebeesthoek Radio Astronomy Observatory (HartRAO) is required to achieve a one-arcsecond (″) pointing accuracy to the lunar retroreflectors (Combrinck, 2014). Key to the achievement of this accuracy is the analysis of the thermally-induced displacements of the HartRAO LLR composite structure (especially the tube assembly) for their possible impact on the pointing accuracy of the telescope. So far, the spatial and temporal analyses of the thermal behaviour of the LLR telescope in relation to the ambient air temperature (denoted as T_{∞}) at the HartRAO site have already been conducted (Tsela et al., 2016a; Tsela et al., 2016c). This is in fact the first study to report on the analysis of the thermally-induced displacements of the HartRAO LLR tube structure that are based on the tube-sensor acquired temperatures with respect to T_{∞}. Therefore, the aim of this study was to estimate the extent of the thermally-induced displacements of the HartRAO LLR optical tube to determine the extent of the correction required to be fed into the steering and pointing model of the LLR telescope (Combrinck, 2014), and in so doing, to counteract the expected thermally-induced pointing offsets. In particular, the correction of the thermally-induced pointing offsets is important for maximizing the pointing accuracy of the telescope, thereby increasing the chance that these pointing offsets are accurately focused on the retroreflectors located on the lunar surface (Tsela et al., 2016b).

2. Brief overview of the laser ranging concept

In principle, laser ranging refers to the firing of ultrashort laser pulses from a source fixed at a particular location to a cube retroreflector mounted on a distant entity. In space geodesy, laser ranging is a technique used for acquiring accurate distance measurements between a particular Earth-based reference station and a fixed reference point (retroreflector arrays) on an orbiting satellite or the Moon surface (Pearlman et al., 2019). The main basic tools used in space geodesy for acquiring accurate distance measurements are widely known as Satellite Laser Ranging (SLR) and LLR. In particular, these tools make use of: (i) ultrashort laser pulses for ranging to the retroreflector arrays, (ii) optical receivers and photon detectors to record the light photons returned to the laser ranging station, and (iii) timing systems to measure the round-trip travel time of the laser pulses from the ground-based station to the optical retroreflectors on an orbiting satellite or the surface of the Moon (Bender et al., 1973).

The International Laser Ranging Service (ILRS) coordinates SLR and LLR data and ensures the successful delivery of the data to a global user community (Pearlman et al., 2019) - key to generating a wide range of geodetic products (Altamimi et al., 2016). For example, the available empirical findings based on analyses of long-term LLR data revealed the slow annual recession rate of the Moon's orbit by approximately 3.8 cm away from the Earth as a result of tidal friction (Murphy, 2013). In addition, the LLR data provide a unique opportunity to test the temporal changes in the Newtonian gravitational constant, G. These changes in G are constrained to $(2\pm7)\times10^{-13}$ per year which indicates the stability of the universal force of gravity (Williams et al., 2004; Müller and Biskupek, 2007).

3. Methodology

3.1. Equipment used

Different instruments were used for measuring the tube temperature of the telescope and the thermally-induced displacements of the LLR optical tube (Table 1). The instruments used in conducting the experiment included (i) Resistant Temperature Detectors (RTDs), which were mounted onto the tube surface by means of a thermal adhesive; (ii) a 12-core shielded communications cable for connecting the RTDs to a data acquisition unit; (iii) the MAQ®20 Modular Data Acquisition System, for the real-time logging of the tube temperature, as measured by the mounted RTDs, and (iv) a total station and prisms for the precise measurement of the LLR tube displacements. Sensor placement, including the two last-mentioned instruments, is discussed in subsequent sections.

Table 1. Summary of equipment used in the analysis of the thermally-induced displacements of the LLR optical tube

	Sensors	**Thermal adhesive**	**Total Station**	**Prisms**	**MAQ®20 Modular Data Acquisition System**	**Wiring**
Description	100 Ω Platinum RTDs (F2020–100–A)	OB–200 epoxy adhesive	Leica Nova MS50 Multi-Station	Leica GPH1P Prism Precision Reflector	Six-channel RTD31 module	12-core shielded cable
Selected properties	Accuracy: ± 0.5 °C; temp. range: -100 to +100 °C	Thermal conductivity *k*: 1.38 W/(m.K)	Laser distance measurements of 1.5 m up to 10,000 m at an accuracy of 1 mm + 1.5 parts per million (ppm)	The centering accuracy of 0.3 mm (which relates to the optical centre of the prism) at a range distance of up to 3500 m	Accuracy: ± 0.12 °C	Resistance: 1.77 Ω ±0.8% distance: 9.4m

3.2. Placement of sensors on the tube

A total of 64 RTDs were systematically arranged and thermally bonded on the first layer surface of the tube (Figure 1). The illustration in Figure 1 (Tsela et al., 2016a) was instrumental in the positioning, labeling and troubleshooting of the RTD sensors. The arrangement of sensors on the tube is such that they are equally spaced and as dense as possible in order to obtain a representative distribution of the temperature and the thermal variations of the tube structure relative to T_{∞}.

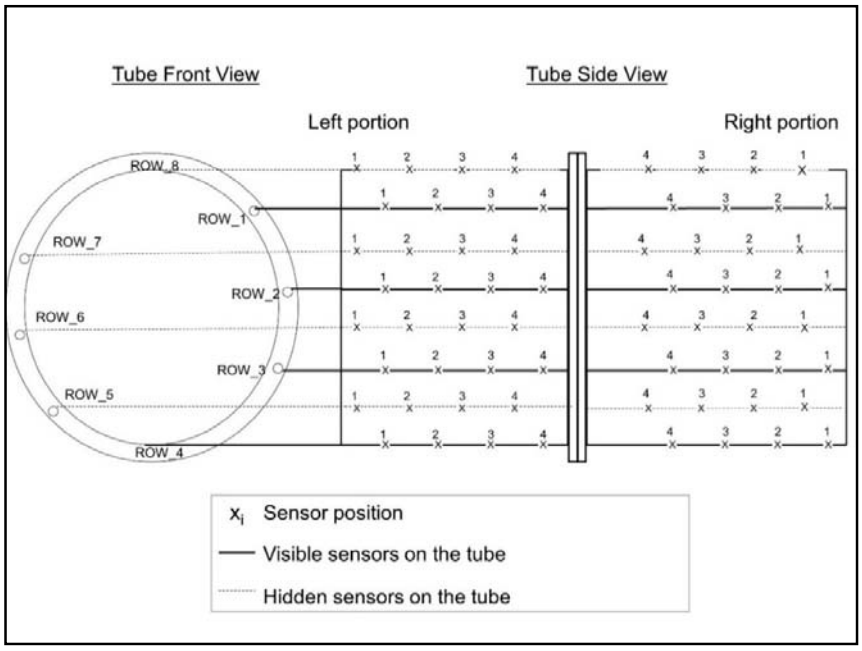

Figure 1. Placement of temperature sensors (RTDs) on the ~3 m LLR optical tube structure. The distance between the sensors along the tube is approximately 140 mm, whereas the distance between the rows around the tube is 127.5 mm.

3.3. MAQ®20 industrial data acquisition and control system

The MAQ®20 Modular Data Acquisition System (DataForth, 2017) from Dataforth Corporation was used in this study for the real-time logging of temperature measurements from the mounted F2020, 100 Ω Platinum RTDs (Table 1). This system takes in a set of RTD31 modules, each with six input channels and has a module-dependent systemic accuracy of ±0.0035%. These modules support both the two- and three-wire RTD configurations. In particular, the three-wire configuration was used for wiring a set of four F2020 sensors per row, per portion of the LLR tube (Figure 1), such that each set of four F2020 sensors was connected to each RTD31 module. Furthermore, these RTD31 modules have a patented lead-wire compensation circuit embedded in them to eliminate the effects of wire resistance (DataForth, 2017). For instance, the wiring used in this study (Table 1)

) spans 9.4 m, a distance which has a lead-wire resistance of 1.77 Ω ±0.8%. If not properly compensated, this resistance can offset temperature measurements by approximately 4.6 °C.

3.4. Multi-station and prism precision reflectors

The Leica Nova MS50 Multi-Station (Figure 2) manufactured by Leica Geosystems is an instrument for measuring, calculating, and capturing distance and angle data (Geosystems, 2013). In this study, the multi-station was used to conduct the laser distance measurements to the prism reflectors (Figure 3). The ranging or distance measurement was conducted through the emission of a visible laser beam (centred at 658 nm) from the multi-station telescope and at a maximum average radiant power of 0.33 mW. In this study, the prism reflectors (Figure 3) were set up to point directly at the multi-station. Four Leica GPH1P Prism Precision Reflectors (Geosystems, 2010b; Geosystems, 2010a) were used for the setup.

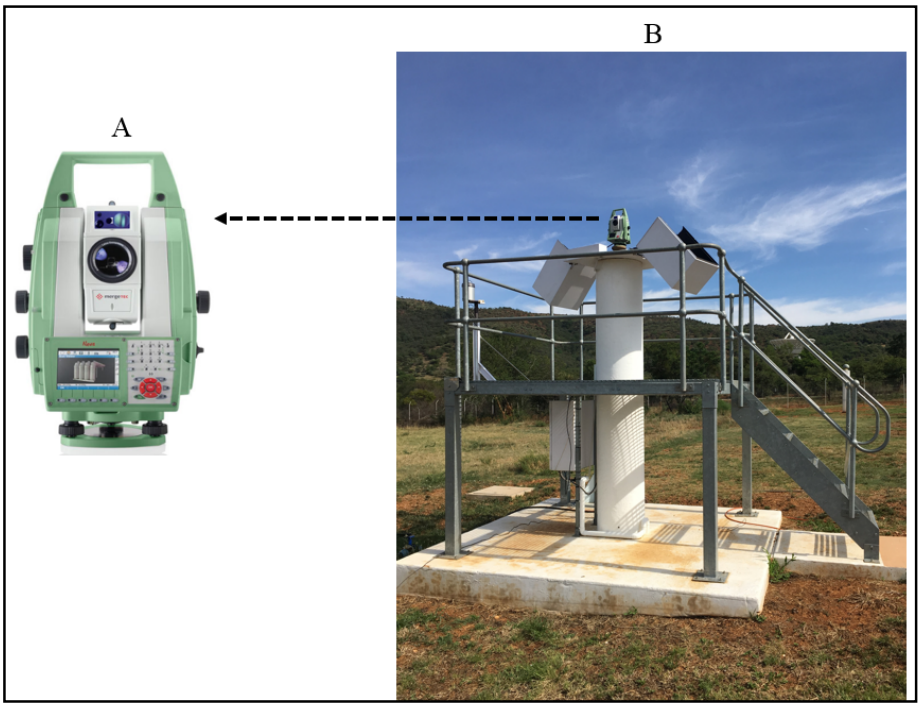

Figure 2. Leica Nova MS50 Multi Station (A), based in HartRAO (B) was used to monitor coordinate displacements (i.e. the northing, easting and height of the GPH1P retroreflectors mounted on the Lunar Laser Ranger tube structure).

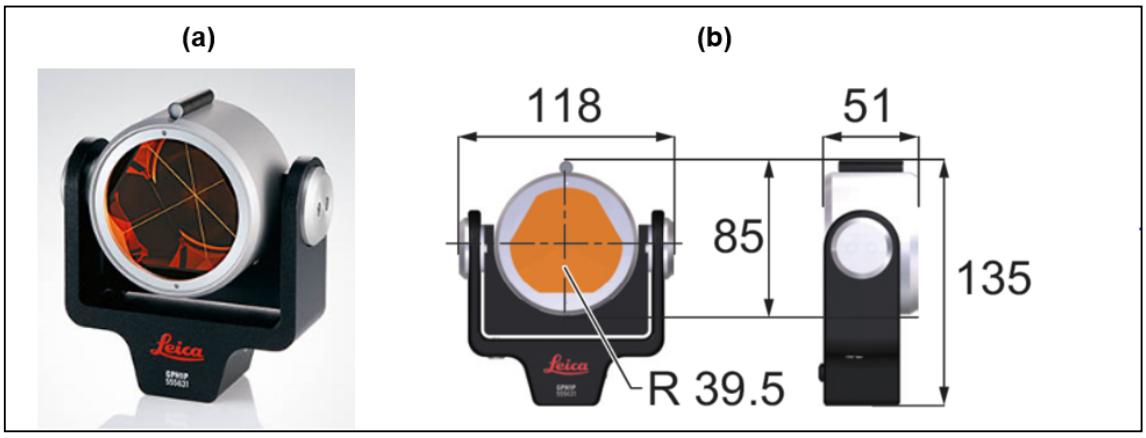

Figure 3. (a) The Leica GPH1P Prism Precision Reflector that was used for measuring coordinate displacements and (b) its corresponding dimensions (Geosystems, 2010a).

3.5. Tube experiment setup

Figure 4 displays the tube experiment setup at HartRAO. It comprises the LLR tube structure and 64 RTD sensors for the acquisition of the real-time temperature measurements of the tube. This experiment setup was based primarily on the procedure, as adopted from Tsela et al. (2016a), and described earlier in Figure 1.

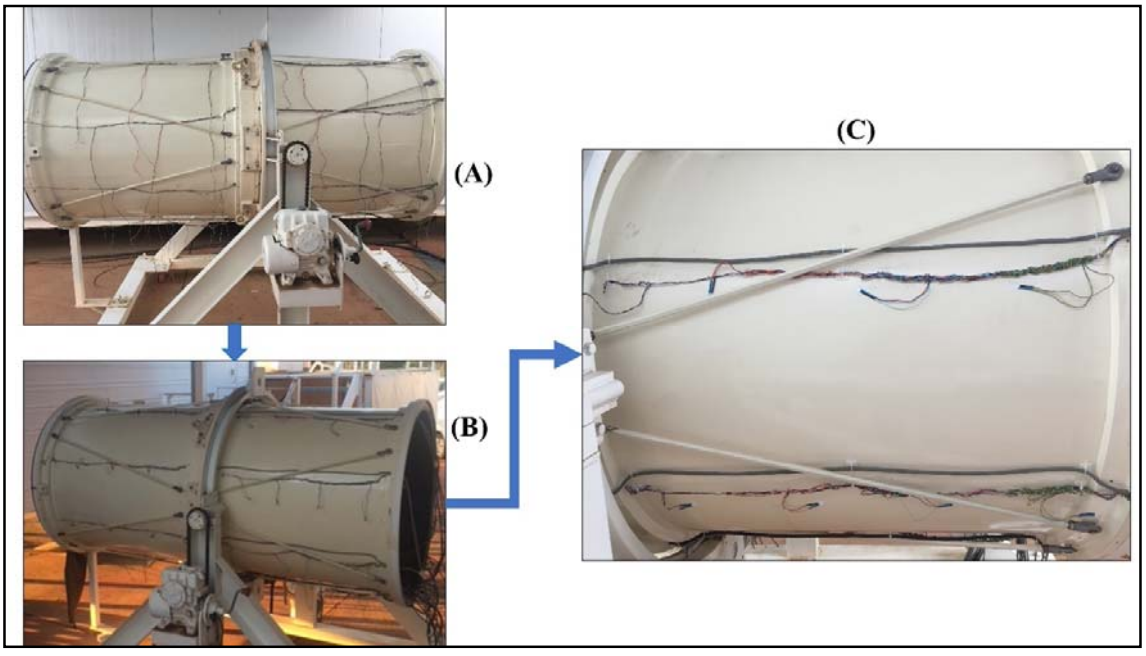

Figure 4. Sensor wiring arrangement (A) and mounted RTD sensors (B) on the first-layer surface of the LLR optical tube at HartRAO. The LLR tube on the metal stand that supports the experimental setup of the LLR tube. For legibility, an expanded view of the mounted RTD sensors is visible on the tube (C).

The LLR tube, mounted with sensors and covered with arc-metal sheets, was integrated into the structural body of the telescope (Figure 5) in order to investigate the relationship between the tube temperature and the temperature-induced tube displacements. Note that on account of the ongoing refurbishments, the internal components of the LLR tube, such as the mirrors, back plate and spider assembly, could not be integrated into the tube structure. The integration of the outstanding internal components will take place as soon as the refurbishments have been completed. This will help in future experiments to produce more realistic indications of thermally-induced tube displacements.

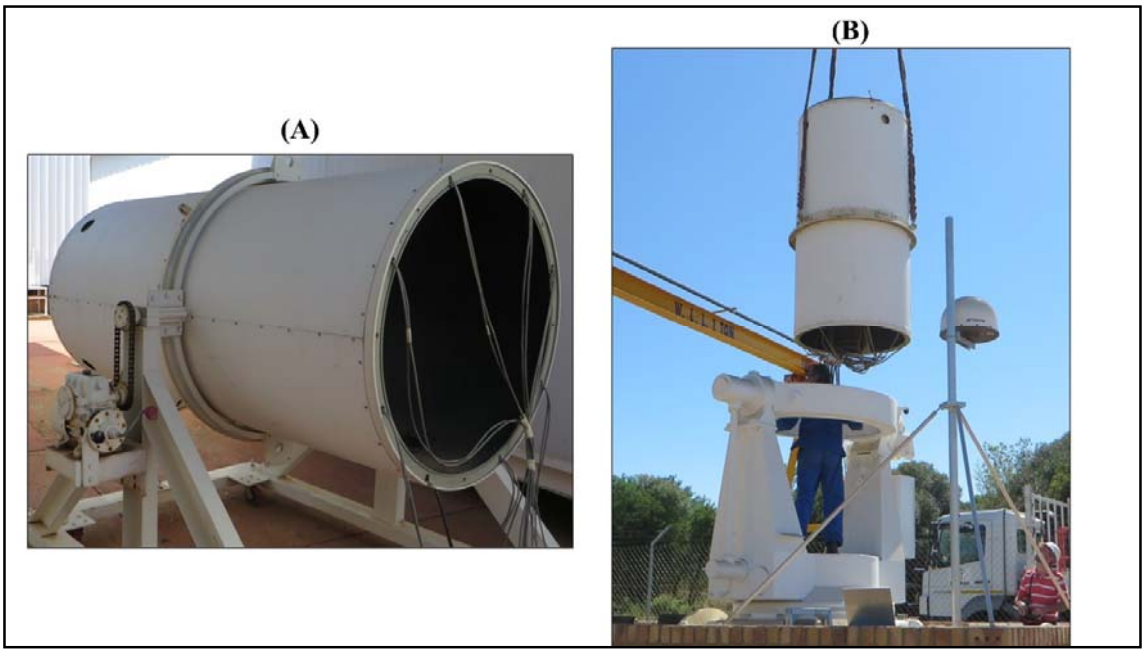

Figure 5. The arc-metal sheets used to cover the mounted sensors on the LLR tube (A). These sheets insulate the tube, as well as the sensors and protect it from external disturbances such as exposure to direct sunlight and wind. The LLR tube integrated into the telescope's elevation and azimuth mount at HartRAO (B). Note that the small circular openings on the front-end of the tube cover sheets indicate the relative locations of the fans which are normally installed for such an experiment.

3.6. Thermally-induced tube displacements

The use of four prisms, as shown in Figure 6, provided information on the relative displacements taking place at different parts of the telescope. For example, the prism mounted on the base structure was used to monitor the stability of the base structure of the telescope and

to distinguish between the displacements caused by the stability of the base structure and those caused by T_∞. The tube was parked at an elevation of about 30° (facing the multi-station) so that any tube displacements in the x, y and z directions could be measured.

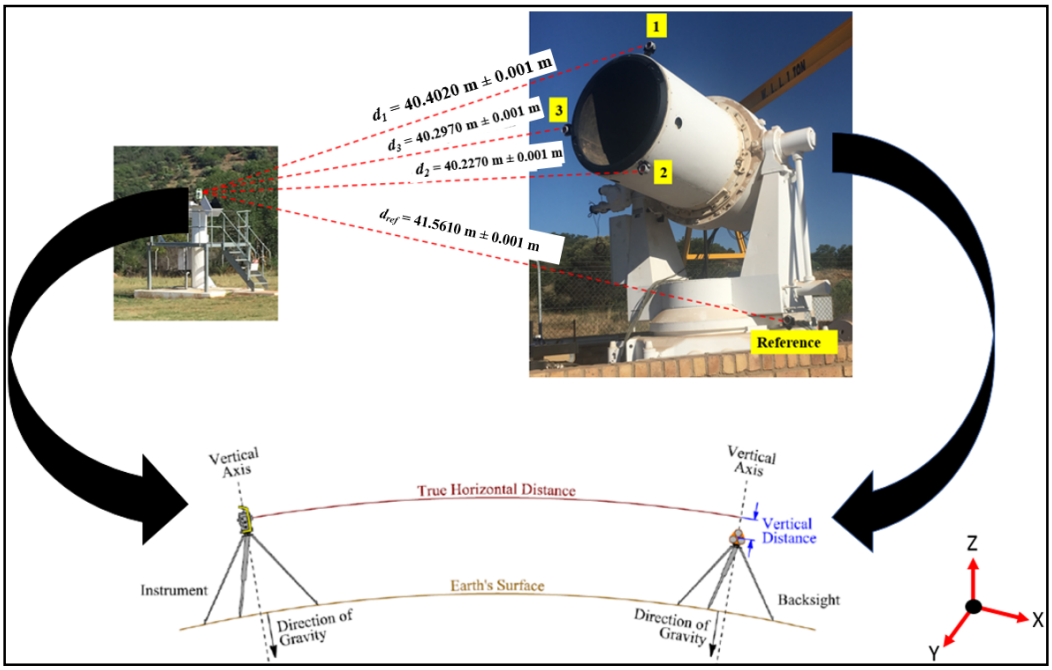

Figure 6. Illustration of the LLR tube displacement monitoring experiment based on the site-based Leica Nova MS50 Multi-Station and the four Leica GPH1P Prism Precision Reflectors mounted on the tube front and base of the telescope. The horizontal distance (d_i) ± the accuracy of the total station measurement between the multi-station and the respective prisms mounted on the telescope are shown in the figure. Theoretical representations of the Earth's curved surface and the parallel horizontal distance are also shown (Torge and Müller, 2012).

The 3-D coordinate displacements from each of the four prisms were automatically logged for two successive days. The telescope (Figure 6) was kept unsheltered over this period and the only temperature variations recorded were due to the day and night ambient temperatures, as well as to cloud cover and natural sunlight. This setup aided efforts to determine the extent of the thermally-induced tube displacements at five-minute intervals during the day and at night (Figure 6). Virtually similar studies (e.g. Hu et al. (2015)), also based on laser alignment systems, have been successful in measuring the extent of an object's displacement and in determining strategies to compensate for such displacements. Furthermore, the optical tube displacements issuing from thermal expansion or deformation have been shown elsewhere (Mittag et al., 2008) to be detrimental to telescope-pointing accuracy. In particular, the output

of this experiment could be an important parameter in the precise determination of the extent of the thermally-induced pointing error arising from the LLR tube to the effect that the error can be compensated for in the LLR pointing model currently under construction (Combrinck, 2014) or through a micro-controller ventilation system.

4. Results and discussion

4.1. LLR tube RTD measurements

Figure 7 illustrates the daily temperature variations of the LLR tube and T_∞ at the HartRAO site that were sampled every five minutes for two successive days (i.e., 30 Nov 2018 – 01 Dec 2018). The LLR tube measurements were averaged from a distribution of 64 RTD sensors and sampled every five minutes. It is evident from Figure 7 that the average temperature of the tube closely follows variations in T_∞ successively during the day and at night. In particular, the average temperature of the tube changed by approximately 0.71 °C after every 30 minutes over the time period considered (Figure 7). As discussed in Tsela et al. (2016a) and Tsela et al. (2016c), such a thermal response time for the tube is largely due to the thermal properties of the tube material, coupled with the heat transfer mechanisms operating on the tube. For example, during the day, the solar radiation effect on the tube is evident in that the average temperature of the tube rises above 30 °C, which is at least four degrees higher than T_∞, especially between 10h00 and 17h00 (Figure 7). If it were not for the double-layer structural design of the tube (Tsela et al., 2016a) which insulates the inner surface or first layer of the tube where the RTD sensors are mounted, this temperature might have increased further.

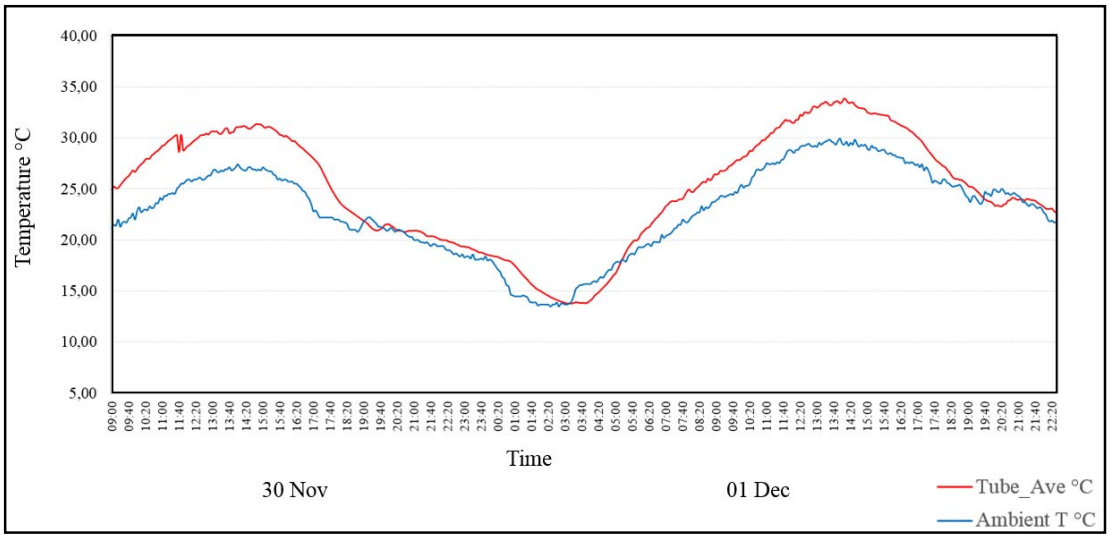

Figure 7. Illustration of the measured average temperature of the LLR tube (Tube_Ave °C) and the ambient air temperature (T_∞) for HartRAO, sampled every five minutes for the times and days shown

During the night, particularly from around 19h00 to the late night hours, the tube temperature and T_∞ generally overlap. This could be due to the ambient temperature stability or the micro T_∞ variations at those times which enable the tube structure to assume an isothermic thermal behaviour (Tsela et al., 2016a). The resulting nighttime discrepancy between tube temperature and T_∞ at the considered times can be expected to be as low as ~1° C. Therefore, nighttime is ideal for the whole tube structure to present with an overall temperature variation of ~1° C. Overall, these findings constitute an important input for the analysis of tube displacements owing to its temperature fluctuations.

4.2. Analysis of relative displacements of the LLR tube

The measured displacements by the reference prism mounted on the telescope base structure were deducted from the measured displacements by the three prisms mounted on the front end of the LLR tube. The subtraction process basically removed the contribution of the base structure displacements from the measured displacements on the tube in respect of height (z), easting (x) and northing (y), respectively. As a result, the relative displacements (Δ) of the front end of the tube over two consecutive days (i.e. 30 Nov 2018 – 01 Dec 2018) are presented in Figure 8 , and are coupled with the statistical summary shown in Table 2. For example, to work out the displacements, all the coordinates (i.e., northing (y) and easting (x) of each prism (i.e.,

1, 2, 3) and the reference prism were recorded. To monitor the magnitude of the changes (Δ) in x and y for the different time intervals, the difference in the northing values was calculated, for example, for Prism 1 and the reference prism, and similarly, also the difference in the easting values for Prism 1 and the reference prism. These differences are summarized in Table 2 in terms of their minimum, maximum and mean values; and expressed under the columns Δ northing [m] and Δ easting [m]. Lastly, the standard deviation was calculated to determine the average deviations at, for example, Prism 1 in the northing (y) and easting (x) directions. As measured by the total station, the average deviations indicate the displacement at Prism 1. The same explanation applies to prisms 2 and 3.

Notable changes are evident in Figure 8 (a) in the relative height displacements of the tube, measured simultaneously in prisms 1, 2 and 3 over the two-day period when the experiments were conducted. The temporal oscillations of the relative displacements of the tube in the vertical direction are evident across both day and night. As a result, these oscillations may be attributed to possible structural changes owing to the variations in temperature (discussed in the next subsection) that the tube is subjected to. For example, the relative displacements on average at prisms 1, 2 and 3 in the vertical direction were 2.5540 ± 0.0007 m, 1.3750 ± 0.0008 m and 1.9780 ± 0.0007 m, respectively (Table 2). The values of 2.5540 m, 1.3750 m and 1.9780 m refer to the vertical heights or distances measured from the centre of the reference prism to the centre of prisms 1, 2 and 3 on the tube, respectively. The corresponding standard deviation values of ±0.0007 m, ±0.0008 m and ±0.0007 m denote the average deviations that occurred in the vertical direction at the centre of prisms 1, 2 and 3, respectively. Therefore, these deviations are referred to as displacements and indicate the changes in the vertical direction from the centre of each prism that were measured by the total station. A difference is noted in the slightly higher standard deviation (hereafter denoted as SD) in respect of the relative displacements at Prism 2. As such, as shown in Nkosi et al. (2016), gravity-induced deformation on the lower arc of the tube front may have had an effect.

The generally higher SD of relative displacements of the LLR tube in the vertical direction rather than in the easting and northing directions (Table 2) suggest that the tube experienced greater variations in the vertical direction, and as a result, those relative displacements could potentially be the largest contributor to the instability of the tube during pointing. Furthermore, the exposure of the tube front to the downward solar irradiance and T_{∞} (particularly during the day) could have implications for the stability of the spider assembly and alignment of the optical axis (Mittag et al., 2008). However, telescopic pointing experiments would have to be

conducted to investigate the significance of the reported relative displacements on the required pointing accuracy in the case of the LLR HartRAO telescope.

Figure 8 (b) reveals the relative displacements of the tube in the easting (x) direction, as measured simultaneously at prisms 1, 2 and 3 over the two-day period when the experiments were conducted. On average, the magnitude of the relative displacements of the tube in the easting (x) direction appeared lowest (compared to both the vertical and northing directions) at 0.0880 ± 0.0005 m, 0.1660 ± 0.0004 m and 0.7380 ± 0.0005 m, corresponding to prisms 1, 2 and 3, respectively (Table 2). The relatively low SD suggests that the tube experienced little variation in the easting direction; thus, throughout the two-day period, it remained more stable in the easting direction than in any other direction.

Furthermore, in Figure 8 (c), the temporal oscillations of the relative displacements in the northern (y) direction are more evident during the day-time when the tube is exposed to incidental solar radiation, and less, especially in respect of Prism 2, during the late afternoon through to the night. On average, the relative displacements at prisms 1, 2 and 3 in the northing (y) direction were 1.2760 ± 0.0005 m, 1.4200 ± 0.0007 m and 1.9060 ± 0.0005 m, respectively (Table 2). While these relative displacements compared favourably with those in the vertical direction, it is interesting to observe that the relative displacements (northing) at Prism 2 presented with higher magnitudes than those at Prism 2 (vertical). Notwithstanding this observation, the relative tube displacements in the northing direction showed little variation. Comparable to the easting direction, this could be an indication that the tube was more stable in the northing and easting directions than in the vertical direction (Table 2).

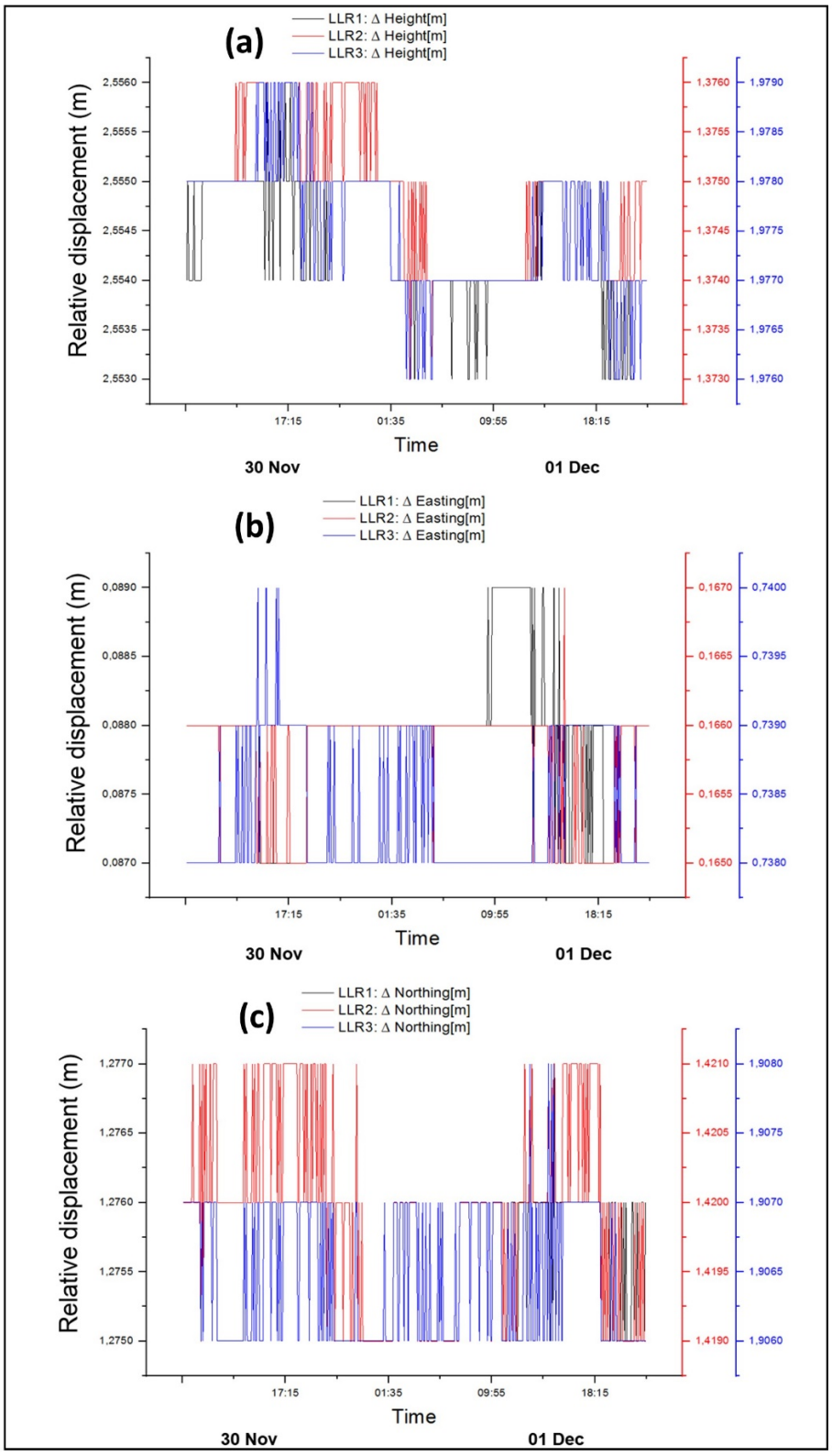

Figure 8. Displacements of the tube, as sampled every five minutes in the vertical (a), easting (b) and northing (c) directions, and relative (Δ) to the base structure of the tube. LLR 1, 2 and 3 denote the respective positions of the three prisms mounted on the front end of the tube.

Table 2. Statistical summary of measured relative tube displacements (Figure 8)

	LLR1: Δ Easting [m]	LLR2: Δ Easting [m]	LLR3: Δ Easting [m]	LLR1: Δ Northing [m]	LLR2: Δ Northing [m]	LLR3: Δ Northing [m]	LLR1: Δ Height [m]	LLR2: Δ Height [m]	LLR3: Δ Height [m]
Min.	0.0870	0.1650	0.7380	1.2750	1.4190	1.9060	2.5530	1.3730	1.9760
Max.	0.0890	0.1670	0.7400	1.2770	1.4210	1.9080	2.5560	1.3760	1.9790
Mean	0.0880	0.1660	0.7380	1.2760	1.4200	1.9060	2.5540	1.3750	1.9780
Std. Dev.	±0.0005	±0.0004	±0.0005	±0.0005	±0.0007	±0.0005	±0.0007	±0.0008	±0.0007

Interestingly, these findings show that, compared to those of the other prisms in both the easting and northing directions, the SD of relative displacements at Prism 2 in the vertical direction (±0.0008 m) was highest (Table 2). This finding could be an indication of an area on the tube that is subject to greater structural deformation. Considering the location of Prism 2 at the lower arc of the tube front, this finding suggests that as opposed to other areas on the tube front, there could be a combination of thermally-induced (Tsela et al., 2016a) and gravity-induced (Nkosi et al., 2016) deformations occurring concurrently on the tube, thus leading to increased variability. This increased variability is hypothesised to introduce more elevation-pointing offsets than azimuth for the LLR, as it has been shown in other studies that there are strong correlations between ambient temperatures and elevation-pointing offsets, reaching about 10″ during telescope pointing (Mittag et al., 2008).

4.3. Analysis of thermally-induced tube displacements

A visual inspection of the time series of the overlaid (i) measured tube average temperature, (ii) ambient air temperature, and (iii) relative displacements of the tube in height, easting and northing show that the relative displacements evidently occur concurrently with the successive peaks of both the average temperature and the ambient air temperature, T_∞, of the tube (Figure 9 - Figure 11). The observed relative displacements of the tube, especially at prisms 1 and 3 and in all directions, generally showed clear successive peaks corresponding to the average temperature and T_∞ of the tube (Figure 9 - Figure 11). This could partially be attributed to the exposure of the tube to direct sunlight, which (i) transiently (from approximately 07h30 to 10h30 in the morning hours) irradiates the west-facing side of the tube where Prism 3 is mounted, and which (ii) continually (from around 11h00 to 17h30) irradiates the top and east-facing side of the tube where Prism 1 is mounted, respectively.

In particular, the relative displacements of tube height (Figure 9) revealed a clearer pattern of oscillation in relation to the average temperature of the tube. Furthermore, the relative displacements of tube height (especially in Figure 9 (a) and (c)) show oscillations that correspond with increases and decreases in the average temperature of the tube, particularly during the times, 15:00 – 22:35 (30 Nov) and 12:40 – 22:00 (01 Dec).

A similar pattern is also evident for relative displacements of the tube toward the east (in Figure 10 (b) and (c)), particularly during the times, 11:45 – 18:15 (30 Nov) and 13:45 – 20:15 (01 Dec). Virtually across the entire time series, the relative displacements of the tube towards the north in Figure 11 (b) presented with the finest oscillations in relation to the tube's average temperature profile. On average, the smallest to largest relative displacements of the tube, measured as ± SD, were in the following order per prism: LLR 1 Δ: 0.0880 ± 0.0005 m (easting), 1.2760 ± 0.0005 m (northing) and 2.5540 ± 0.0007 m (height); followed by LLR 3 Δ: 0.7380 ± 0.0005 m (easting), 1.9060 ± 0.0005 m (northing) and 1.9780 ± 0.0007 m (height); and LLR 2 Δ: 0.1660 ± 0.0004 m (easting), 1.4200 ± 0.0007 m (northing) and 1.3760 ± 0.0008 m (height). These findings indicate that the tube undergoes structural changes (expansion and contraction) concurrently with changes in temperature and that the uneven displacements of the tube in three directions are associated with its closer proximity to the area where the spider assembly is mounted.

This information could be used as a guideline to determine the extent of the corrective inputs to be fed into the LLR telescope pointing model (Combrinck, 2014) to counteract thermally-induced pointing offsets. The general idea would be to ensure an even distribution of temperature throughout the telescopic tube (and its mounted assembly) through a microprocessor-controlled venting system. This would apply especially to those areas where mechanical distortion would lead to errors in optical collimation, alignment and focusing (e.g., in the secondary mirror spider assembly), which should in fact not be unevenly heated.

It is worth mentioning that the measurements acquired in this study to produce the relative displacement results, were automatically corrected for natural errors by the Leica Nova MS50 Total Station (Geosystems, 2013). This station compensated for the environmental conditions at the site and for the curvature and refraction constants applied to each measurement (Geosystems, 2013). When calculating the horizontal and height differences, these constants were applied to compensate for the curvature of the Earth and atmospheric refraction.

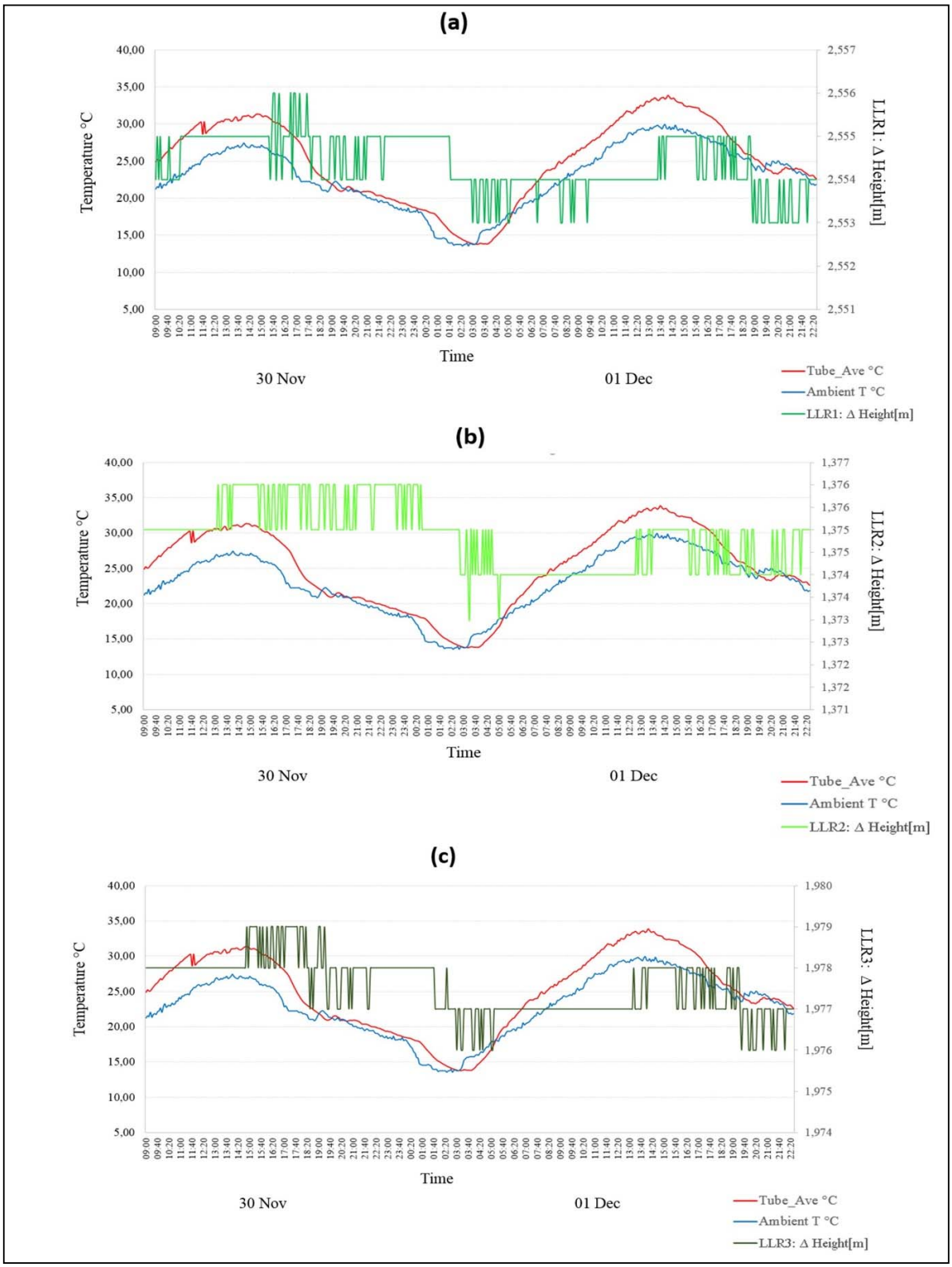

Figure 9. Time series of the tube's measured average temperature and ambient air temperature and the relative displacements of tube height at the location where the LLR prisms 1 (a) ,2 (b) and 3 (c) prisms were mounted.

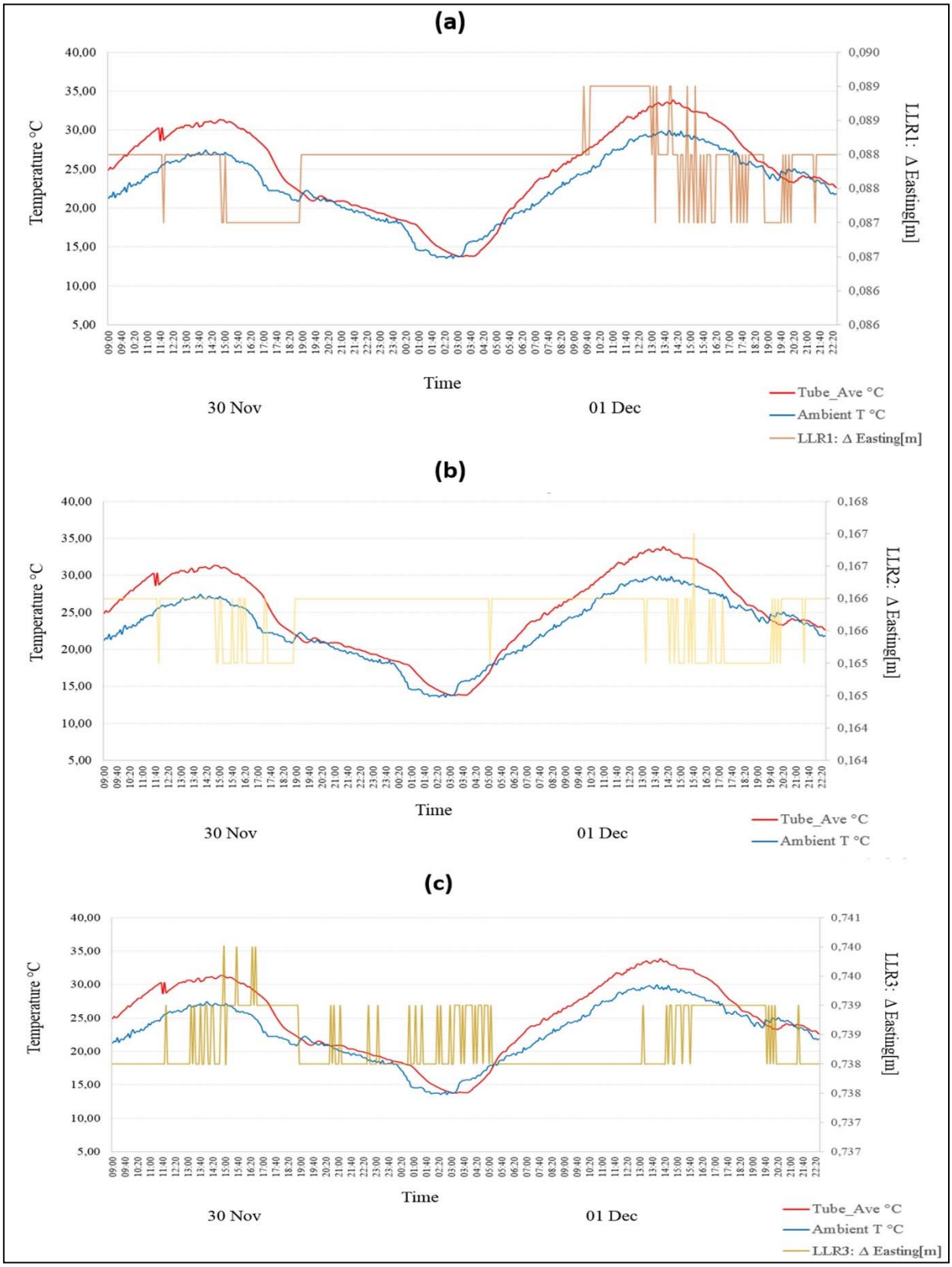

Figure 10. Time series of the tube's measured average temperature and ambient air temperature and the relative displacements of the tube toward the east at the location where the LLR prisms 1 (a),2 (b) and 3 (c) prisms were mounted.

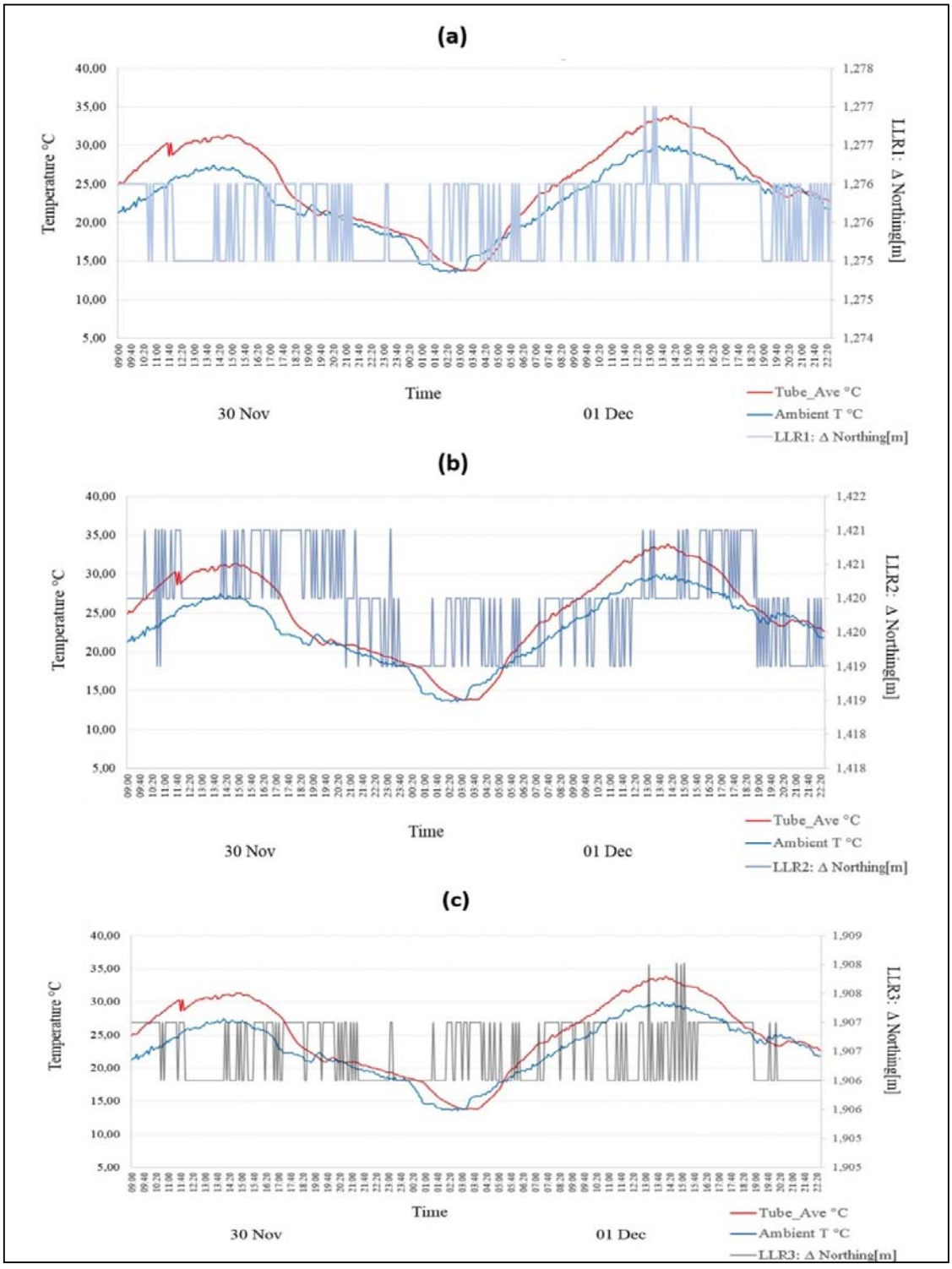

Figure 11. Time series of the tube's measured average temperature, ambient air temperature and the relative displacements of the tube toward the north at the location where the LLR prisms 1 (a), 2 (b) and 3 (c) were mounted.

5. Conclusion

This study showed that while the optical tube undergoes structural changes (expansion and contraction) in association with changes in temperature, the position of the tube in closer proximity to the place where the spider assembly is mounted results in the uneven displacement of the tube in three directions. For the time period considered in this study which was characterized by T_{∞}, that varied between 11.20 °C and 29.90 °C, and that was characterized by corresponding tube average temperatures that varied between 13.75 °C and 33.84 °C, it was found that on average, the smallest to largest relative displacements measuring ± SD for the tube were in the following order per prism: LLR 1 Δ: 0.0880 ± 0.0005 m (easting), 1.2760 ± 0.0005 m (northing) and 2.5540 ± 0.0007 m (height); followed by LLR 3 Δ: 0.7380 ± 0.0005 m (easting), 1.9060 ± 0.0005 m (northing) and 1.9780 ± 0.0007 m (height); and LLR 2 Δ: 0.1660 ± 0.0004 m (easting), 1.4200 ± 0.0007 m (northing) and 1.3760 ± 0.0008 m (height). As the precision of the total station used for the measurements is at the 1 mm level, these figures are just an indication of displacement. However, owing to its high sampling rate, it is possible to provide statistical sub-mm ranges.

Furthermore, comparable to the easting direction, the relative displacements of the tube in the northing direction showed little variation, this could thus be an indication that the tube is more stable in the northing and easting directions than in the vertical direction. Additionally, the SD of relative displacements at Prism 2 in the vertical direction was highest (±0.0008 m) as opposed to that of the other prisms in both the easting and northing directions. This finding could be an indication of the area on the tube that is subjected to greater structural deformation. Considering the location of Prism 2 at the lower arc of the tube front, this finding suggests that as opposed to other areas on the tube front, there could be a combination of thermally and gravity-induced deformations occurring concurrently on the tube, and as such, leading to increased variability. As demonstrated elsewhere in other studies (Mittag et al., 2008), this increased variability is hypothesised to introduce more elevation pointing offsets than azimuth for the LLR,. This information could be used as a guideline to determine the extent of corrective inputs needed to be fed into the LLR telescopic pointing model (Combrinck, 2014) to counteract the thermally-induced pointing offsets. This is imperative in maximizing the pointing accuracy of the telescope, thereby increasing the chance of it being on-target in focusing on the retroreflectors located on the lunar surface.

The general idea would be to ensure an even distribution of temperature throughout the telescopic tube and its mounted assembly. There should be no unevenly heated areas, especially

where mechanical distortions would of necessity lead to errors in optical collimation, alignment or focusing, as in the case of the secondary mirrored spider assembly. Up to this point in time, Combrinck (2014) has operated a prototype pointing and steering software package on a 125 mm dual refractor testbed telescope and achieved RMS error values at the 0.5″ level. It will be interesting to observe the extent of the variation in the attained values, particularly when the pointing model is tested on the actual LLR telescope, which, during its operation, will be exposed to a varying thermal environment.

Lastly, this study demonstrated that as opposed to the traditional approaches, the laser alignment system can be regarded as an alternative method (Bremer and Penalver, 2002; Greve et al., 2005; Murphy Jr et al., 2008) for detecting and measuring the extent of object displacements, particularly of the telescope's critical components as they undergo varying disturbances (e.g., thermal expansion or deformation) triggered by the local climatic environment.

Acknowledgement

P. L. Tsele hereby acknowledges research support in part by the National Research Foundation of South Africa for Unique Grant No. 93952. Any opinions, findings, conclusions, or recommendations expressed in this material are solely those of the authors. As such, the NRF does not accept any liability in this regard. Furthermore, the authors express their gratitude to the Inkaba yeAfrica project, the Department of Science and Technology of South Africa, and the HartRAO for their support.

References

Altamimi, Z., Rebischung, P., Métivier, L. & Collilieux, X. 2016. ITRF2014: A new release of the International Terrestrial Reference Frame modeling nonlinear station motions. *Journal of Geophysical Research: Solid Earth,* 121**,** 6109-6131.

Baars, J., Hooghoudt, B., Greve, A. & Penalver, J. 1988. Thermal control of the IRAM 30-m millimeter radio telescope. *Astronomy and Astrophysics,* 195**,** 364-371.

Bely, P. 2003. *The design and construction of large optical telescopes*, Springer.

Bender, P., Currie, D., Dicke, R., Eckhardt, D., Faller, J. E., Kaula, W., Mulholland, J., Plotkin, H., Poultney, S. & Silverberg, E. 1973. The lunar laser ranging experiment. *Science,* 182**,** 229-238.

Bremer, M. & Penalver, J. FE model-based interpretation of telescope temperature variations. Workshop on Integrated Modeling of Telescopes, 2002. International Society for Optics and Photonics, 186-195.

Çengel, Y. A. & Ghajar, A. J. 2011. *Heat and mass transfer: fundamentals and applications*, McGraw-Hill.

Cho, M., Corredor, A., Vogiatzis, K. & Angeli, G. Thermal analysis of the TMT telescope structure. SPIE Astronomical Telescopes+ Instrumentation, 2010. International Society for Optics and Photonics, 77380C-77380C-12.

Combrinck, L. Development of a high accuracy, user-friendly Lunar Laser Ranging telescope steering and pointing software package at HartRAO. 19th International Workshop on Laser Ranging, Annapolis, Maryland, 2014.

Cui, C., Feng, Q. & Zhang, B. 2015. Compensation for straightness measurement systematic errors in six degree-of-freedom motion error simultaneous measurement system. *Applied Optics,* 54**,** 3122-3131.

Cui, M., Berg, S. A. & Bhattacharya, N. 2016. Distance measurement in air without the precise knowledge of refractive index fluctuation. *arXiv preprint arXiv:1611.06107*.

Dataforth 2017. The MAQ®20 Industrial Data Acquisition and Control System 2017 Product Catalog. 40.

Énard, D., Maréchal, A. & Espiard, J. 1996. Progress in ground-based optical telescopes. *Reports on Progress in Physics,* 59**,** 601.

Geosystems, L. 2010a. Product Information Prism dimensions 1.

Geosystems, L. 2010b. Surveying Reflectors - White Paper Characteristics and Influences. 13.

Geosystems, L. 2013. Leica MS50/TS50/TM50 User Manual. 84.

Greve, A., Bremer, M., Penalver, J., Raffin, P. & Morris, D. 2005. Improvement of the IRAM 30-m telescope from temperature measurements and finite-element calculations. *Antennas and Propagation, IEEE Transactions,* 53**,** 851-860.

Greve, A. & Kaercher, H. J. 2009. Performance improvement of a flexible telescope through metrology and active control. *Proceedings of the IEEE,* 97**,** 1412-1420.

Greve, A. & MacCoed, G. 2001. Thermal model calculations of enclosures for millimeter wavelength radio telescopes. *Radio Science,* 36**,** 1111-1128.

Hu, P., Mao, S. & Tan, J.-B. 2015. Compensation of errors due to incident beam drift in a 3-D OF measurement system for linear guide motion. *Optics Express,* 23**,** 28389-28401.

Mittag, M., Hempelmann, A., Gonzalez-Perez, J. & Schmitt, J. 2008. The Temperature Dependence of the Pointing Model of the Hamburg Robotic Telescope. *Publications of the Astronomical Society of the Pacific,* 120**,** 425-429.

Müller, J. & Biskupek, L. 2007. Variations of the gravitational constant from lunar laser ranging data. *Classical and Quantum Gravity,* 24**,** 4533.

Murphy Jr, T., Adelberger, E. G., Battat, J., Carey, L., Hoyle, C. D., Leblanc, P., Michelsen, E., Nordtvedt, K., Orin, A. & Strasburg, J. D. 2008. The Apache point observatory lunar laser-ranging

operation: instrument description and first detections. *Publications of the Astronomical Society of the Pacific,* 120**,** 20-37.

Murphy, T. 2013. Lunar laser ranging: the millimeter challenge. *Reports on Progress in Physics,* 76**,** 076901.

Nkosi, N., Combrinck, W. & Akombelwa, M. 2016. Optical configuration and optical tests of the HartRAO Lunar Laser Ranger. *South African Journal of Geology 2016,* 119**,** 99-108.

Pearlman, M. R., Noll, C. E., Pavlis, E. C., Lemoine, F. G., Combrink, L., Degnan, J. J., Kirchner, G. & Schreiber, U. 2019. The ILRS: approaching 20 years and planning for the future. *Journal of Geodesy***,** 1-20.

Pisanu, T., Buffa, F., Morsiani, M., Pernechele, C. & Poppi, S. Thermal behavior of the Medicina 32-meter radio telescope. SPIE Astronomical Telescopes+ Instrumentation, 2010. International Society for Optics and Photonics, 773935-773935-9.

Shinnaga, H., Chamberlin, R., Phillips, T., Dowel, D., Yoshida, H. & Peng, R. 2004. A consideration of thermal effect on pointing measured on a Nasmyth focus of the CSO 10.4 m Leighton telescope at k350 lm. Technical Memorandum.

Torge, W. & Müller, J. 2012. *Geodesy*, Walter de Gruyter.

Tsela, P., Combrinck, L., Botha, R. & Ngcobo, B. 2016a. Thermal analysis of the LLR optical telescope tube assembly based in Hartebeesthoek Radio Astronomy Observatory. *Acta Geodaetica et Geophysica,* 51**,** 393-403.

Tsela, P., Combrinck, W., Botha, R. & Ngcobo, B. 2016b. A proposed mathematical model of thermal variations on the HartRAO Lunar Laser Ranging telescope for enhanced test of Earth-Moon system dynamics. *South African Journal of Geology 2016,* 119**,** 83-90.

Tsela, P. L., Combrinck, L. & Ngcobo, B. 2016c. A spatiotemporal analysis of the effect of ambient temperatures on the thermal behaviour of the Lunar Laser Ranging optical telescope at Hartebeesthoek Radio Astronomy Observatory. *South African Journal of Geomatics,* 5**,** 373-392.

Ukita, N. 1999. Thermal effects on the pointing of the Nobeyama 45-m telescope. *Publications of the National Astronomical Observatory of Japan,* 5**,** 139-147.

Vogiatzis, K. Thermal modeling environment for TMT. SPIE Astronomical Telescopes+ Instrumentation, 2010. International Society for Optics and Photonics, 77380B-77380B-10.

Wang, H., Cheng, J., Lou, Z., Liang, M., Zheng, X., Zuo, Y. & Yang, J. 2018. A comparative study of the thermal performance of the primary mirror at the four typical sites. *Optik,* 174**,** 727-738.

Williams, J. G., Turyshev, S. G. & Boggs, D. H. 2004. Progress in lunar laser ranging tests of relativistic gravity. *Physical Review Letters,* 93**,** 261101.

Wresnik, J., Haas, R., Boehm, J. & Schuh, H. 2007. Modeling thermal deformation of VLBI antennas with a new temperature model. *Journal of Geodesy,* 81**,** 423-431.